MuLan Progress Report 2004

T.I. Banks[1], E. Bartel[5], R.M. Carey[2](Co-spokesman), S. Cheekatmalla[6], D. Chitwood[3], C. Church[5], S.M. Clayton[3], K.M. Crowe[1], P.T. Debevec[3], S. Dhamija[6], M.L. Dantuono[5], W. Earle[2], R. Esmaili[5], A. Gafarov[2], B. Graf[2], F.E. Gray[1], K. Giovanetti[5], T. Gorringe[6], D.W. Hertzog[3](Co-spokesman), P. Kammel[3], B. Kiburg[3], B. Lauss[1], K.R. Lynch[2], R. McNabb[3], Y. Matus[2], J.P. Miller[2], F. Mulhauser[3,8](On site coordinator), C.J.G. Onderwater[7], M. Ojha[6], C.S. Özben[4], Q. Peng[2], S. Rath[6], B.L. Roberts[2], D. Webber[3]

BERKELEY[1] – BOSTON[2] – ILLINOIS[3] – ITU[4] – JAMES MADISON[5] – KENTUCKY[6] – KVI[7] – PSI[8]

January 19, 2005

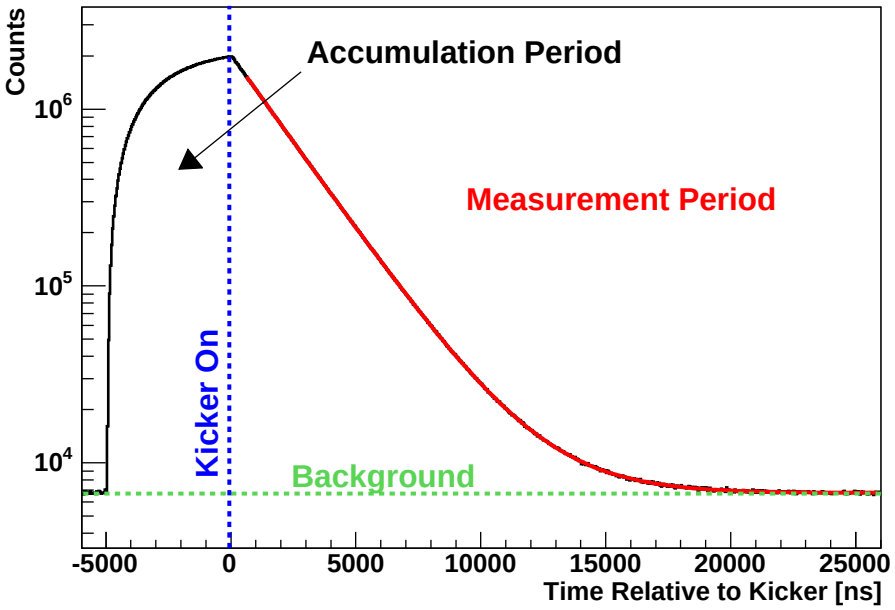

1 Summary

The MuLan Collaboration has had numerous successes in 2004 and two setbacks. Most importantly, we can confidently state that the physics phase of the MuLan experimental program has begun; lifetime data were obtained during a few weeks in December 2004. The Collaboration is largely the same. Two new institutes have officially joined: Kernfysisch Versneller Instituut (KVI) and Istanbul Technical University (ITU). Both include former MuLan colleagues (Onderwater and Özben) who have taken senior positions in their respective home countries. Project Manager Francoise Mulhauser is also now jointly associated with Illinois and PSI under a cooperative agreement between these institutes. Many undergraduate and graduate students continue to participate in MuLan. Several students will obtain their Ph.D. theses based on MuLan data.

Our 2004 successes include:

- The kicker RF emission was largely eliminated after completion of an extensive program of improvements by our TRIUMF engineers. No appreciable noise is now observed in any of our detectors during HV switching.
- Dedicated extinction studies were carried out and final tunes were prepared.
- Measurements of muon stopping range were made by using the MuCap cylindrical wire chambers to map the longitudinal stopping distribution.
- A new high-rate entrance muon chamber (EMC) was built, tested and used in the experiment.
- The full detector ball, EMC, and DAQ system were used for physics data taking.
- A data set having greater than 4×10^{10} positron decays using different targets and data-taking strategies was obtained. Analysis is in progress.

We have also had several disappointments:

- The critical waveform digitizer (WFD) production remains behind schedule. Although we are having success with a new prototype, the running in 2004 relied on a network of conventional discriminators and CAEN multi-hit TDCs.
- The kicker had a number of unexpected failures of its MOSFET cards. The responsible factors are being identified and corrections are being made. Significant disruption to the run reduced data collection time. Additionally, the kickers had to be operated at lower voltage, with a resulting smaller extinction factor.

Due to these problems, we ran at rates 5 times lower than planned.

The Collaboration goals for 2005 include complete analysis of the 2004 data, installation and commissioning of the WFDs, several minor beamtune adjustments, and finally a short physics production run with full WFD electronics installed. Our beamtime request is for 9 weeks total, split into two periods separated by several months. The details are given in the final section of this report.

2 MuLan Experimental Concept

The MuLan experiment is simple in concept. A stream of approximately 20 muons is brought to rest in a thin target during an accumulation period of several microseconds. The muon beam is then "switched off", and decays are recorded by a surrounding detector (the MuLan "ball") during a measuring interval lasting approximately 10 muon lifetimes (22 μs). This cycle is repeated until greater than 10^{12} decays are recorded. The time-structured muon beam must be created artificially at PSI by installation of a new custom kicker. During the measuring interval, the Michel positrons are recorded by a multi-segmented, symmetric detector. The geometry features 170 independent scintillator tile pairs, with each element read out by a PMT whose signal is sampled at 500 MHz by a dedicated waveform digitizer. The time of arrival and energy deposited in each tile are derived from the signal shape. Decay time histograms are constructed from coincident hits and are then fit to extract the lifetime.

The design of the experiment is driven by systematic error considerations. Primary concerns are related to multi-particle pileup, muon spin precession, time-dependence of detector gains or electronic thresholds, and backgrounds. Pileup is minimized by the segmentation of the detector, by the relatively low peak rate per element, and by the double-hit resolution enabled by recording the pulse height in both tile elements for each event. Uncontrolled precession of the stopped, polarized muon ensemble can cause a change in acceptance of the detectors during the measuring interval, which occurs because the emitted positron rate is correlated to the direction of the muon spin. We plan to minimize the residual polarization by using a depolarizing target material, such as sulfur. Further reduction is realized by a dephasing of the initial spins in a magnetic field applied to the target. In addition, a second target material, Arnokrome-3, is used. This material has a high internal field ($\sim$ 0.5 T) which results in very fast precession. Finally, the detector features front-back matched, symmetric segments, where the sum of elements is nearly immune to a change in spin direction.

The instrumentation naturally divides into sub-systems: the muon beam (Illinois); magnets and targets (Berkeley); the detector ball and EMC (Illinois); the calibration system (JMU); the waveform digitizers and clock systems (Boston); and the data acquisition, logging and online analysis computers (Kentucky). Institutions with primary responsibilities for these items are indicated, but much of the work is shared by all collaborators.

3 Beam Studies

The πE3 beam line is run as a linear achromat. Two opposing 60° bends raise the beam up from the level of the cyclotron approximately 5 m to the πE3 experimental area. In the πE3 area a vertical separator, the MuLan kicker, and two quadrupole triplets transport the beam to the center of the MuLan ball. The tune that we have developed for MuLan features a beam with very small divergence in the vertical plane as it passes through the kicker. A second-order Graphical Transport calculation [3] of the MuLan tune is shown in Fig. 1. After the kicker the first triplet focuses the beam onto the selection slits. When the kicker is energized, the beam is kicked down into the slits. The second triplet, which has approximately unit magnification in both planes, focuses the beam onto the target in the center of the MuLan detector. The beam envelope shown in the figure represents approximately the full acceptance of the channel, where the limiting aperture is the 15 cm gap of the kicker. For the fall 2004 run the slits between the two dipoles were used to restrict

the rate to a few MHz with an accompanying reduction in the beam envelope. We have achieved rates as high as 40 MHz when the slits between the two dipoles were opened.

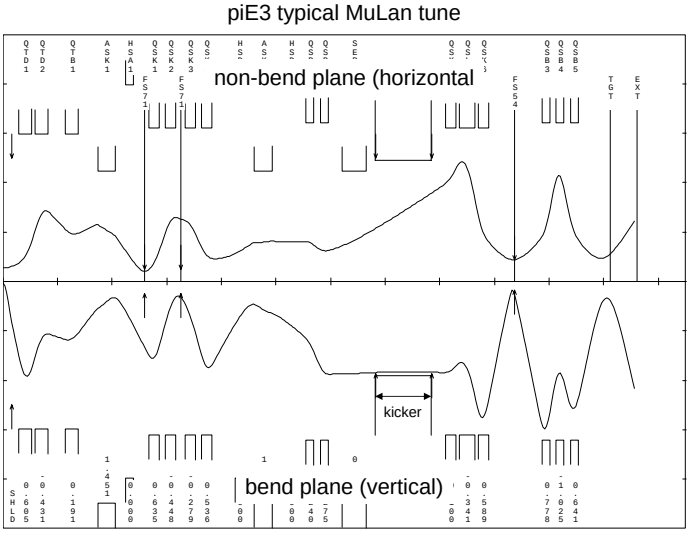

Figure 1: *Second-order Graphical Transport calculation of MuLan tune for the πE3 beam line. In this representation, the muons are emitted from a target on the left side of the panel. The outer envelopes of the beam extent are indicated by the solid line. The individual quadrupoles are indicated by the rectangular shapes, closest to the beam axis. The dipoles are displaced. The electrostatic separator includes a dipole. The kicker region is depicted explicitly. Note the small divergence of the beam in the bend plane through the kicker region. The experiment is located at the final focus, just downstream of the last quadrupole triplet.*

A shortcoming of this tune of is the lack of a dispersed focus at the position of the first set of slits. Surface muons, with a nominal momentum of 29.75 MeV/c, have a range of 140 mg/cm^2 in Mylar. In addition to the vacuum window, the muons must pass through the entrance muon counter (EMC) and a 40 cm long helium bag to reach the stopping target in the center of the detector. Lower momentum muons can easily range out in material upstream of the stopping target because of the strong dependence of range on momentum, $R \propto p^{3.6}$, and range straggling. A variation on our standard tune does produce a dispersed focus in a second Transport calculation, and the Monte Carlo simulation program, Turtle [4], does show improved momentum definition in this modified tune. This improvement has not been verified by our measurements, and our understanding of the momentum acceptance of the πE3 beamline needs improvement.

The MuLan experiment followed the MuCap experiment in fall 2004. The MuCap detector uses two cylindrical wire chambers and a plastic scintillator shell for electron tracking. Before the MuCap detector was removed from πE3, we used the MuCap electron tracking detectors to measure the longitudinal distribution of muons ranging out in air after exiting the πE3 beamline through

the vacuum window. The tracking detectors selected Michel electrons emitted perpendicular to the beam line. The distribution of these perpendicular decays then shows the stopping distribution of the muons. Stopping distributions for kicked and unkicked beam are shown in Fig. 2.

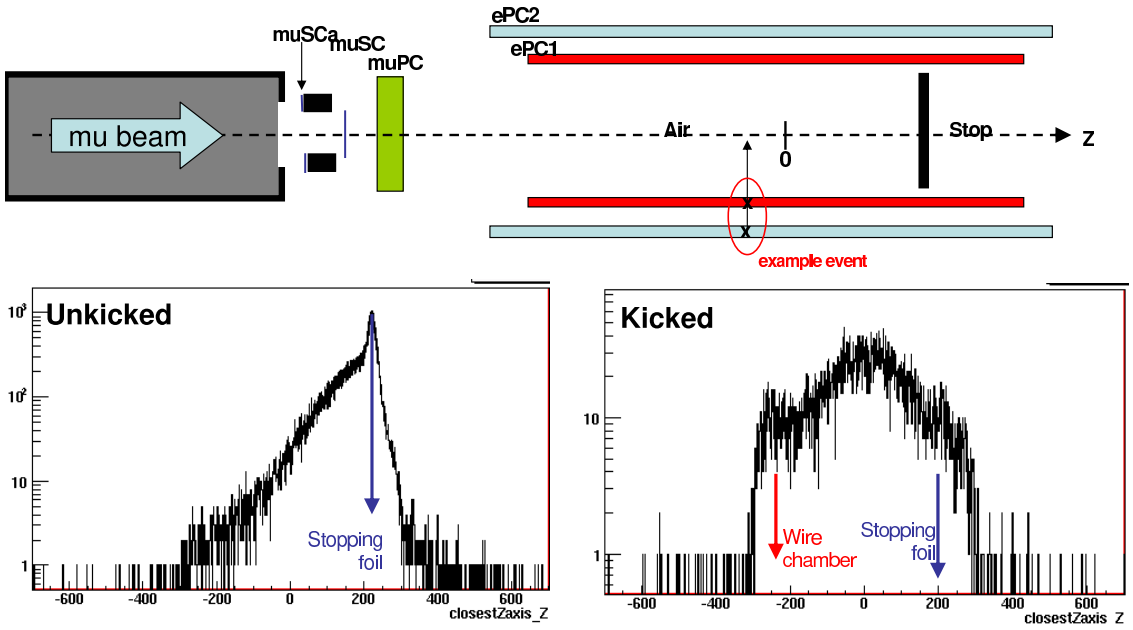

Figure 2: *Top panel shows the generic setup for measuring the muon longitudinal stopping distribution using the MuCap detector. The muon beam leaves the vacuum, passes through a thin scintillator and the MuCap wire chamber (the thickness is similar to our EMC) and then into air. A thin plastic plate is used to stop the highest momentum muons at the exit of the MuCap tracker. The bottom left panel shows the stopping distribution at the nominal momentum f=1.05, which was used in the physics runs. Approximately 1/1000 stop in the foils of our EMC (not visible in this plot). The bottom right panel shows the same distribution with the kicker on, that is, it shows the stopping distribution of those muons that are not kicked away. Note the significant downward shift in mean momentum.*

Higher (lower) momentum muons have a longer (shorter) range. The stopping distribution for a muon of a specific momentum was calculated with the Monte Carlo program, SRIM [5]. These range distributions were then used through a deconvolution to obtain the momentum distribution of the muons. As a final step SRIM was used again to calculate the energy loss and straggling of the muons in the vacuum window, and these distributions were used to infer the momentum distribution of the muons transported by the πE3 beamline. Unfortunately, after the several steps of analysis these range distribution data show little difference between the standard MuLan tune and the tune with improved momentum definition. We must find a different technique to determine the momentum acceptance of πE3. Stopping distribution measurements of the kicked beam appear to show that the kicked beam has, on the average, a lower momentum. A low momentum tail in the momentum distribution at the level of few percent cannot be excluded by our stopping distribution measurements.

The nominal requirement for the kicker is an extinction of the unkicked beam by a factor of

1000 in pulsed mode. This factor has been achieved, but we have found that the extinction factor can easily be reduced by factors of two to five with small changes in the settings of the dipoles, the quadrupoles upstream of the separator, the separator electric and magnetic fields, and the focus achieved by the first triplet at the selection slits. For example, a failure to account for hysteresis in the separator magnet, when resetting the separator after an access, can change the extinction by a factor of two. The rate in a scintillator just downstream of the EMC versus kicker voltage is shown in Fig. 3. The figure shows that the rate begins to level off at a kicker high voltage of 10 kV on each plate, before the maximum voltage on each plate of 12.5 kV. The conservative specification of the kicker voltage and plate length is born out by measurement. Difficulties with the kicker are discussed elsewhere in this report. Despite these difficulties the extinction factor during production running in December, 2004 was between 300 and 400 over a period of about 15 days.

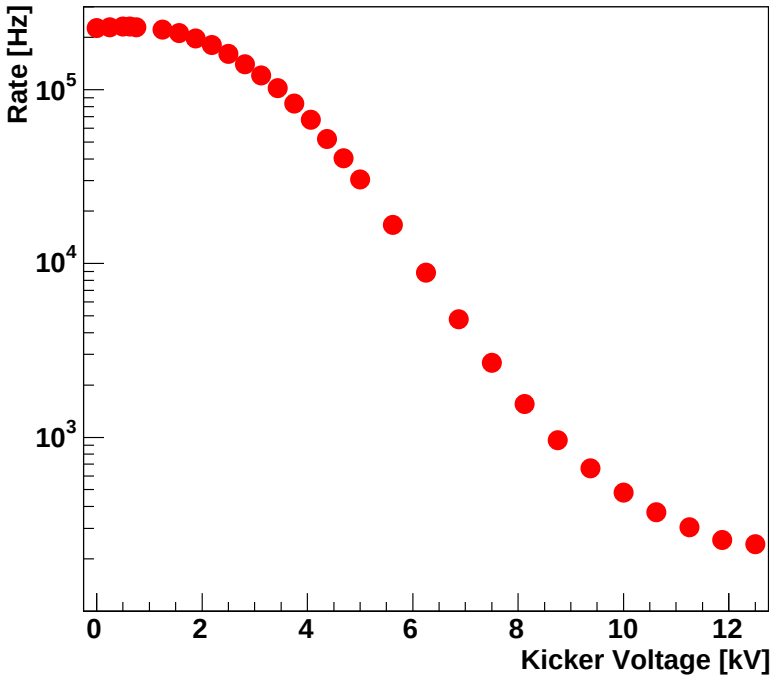

Figure 3: *Muon rate in a scintillator at the entrance of the MuLan detector versus high voltage on the kicker plates. Note that the rate levels off at a high voltage of 12.5 kV.*

The high degree of segmentation and symmetry of the MuLan detector allow a careful investigation of the direction of the polarization vector of the muon beam. This direction is of interest in our estimation of systematic errors due to beam polarization. The positive muon beam(DC mode) was stopped in a 250 μm thick pure silver target. This target does not depolarize the muons. The target was surrounded by an array of permanent magnets in a Halbach configuration [6] which produced a quasi-uniform field of approximately 150 G. Data were taken with the magnet in four orientations. One orientation had the field at an angle of 45° with respect to the beam direction.

The time spectrum of each detector element showed the asymmetry due to the muon spin rotation. The magnitude of the asymmetry depends on the orientation of the detector element with respect to plane of rotation of the spin vector. A global fit of the asymmetry data from the entire detector determines the initial direction of the spin vector to a fraction of a degree. Spin rotation in the field of the separator and the fringe field of the permanent magnet must still be included in the analysis. Preliminary analysis shows that the transverse components of the spin are less than 5% of the longitudinal component.

4 Electrostatic Kicker

The kicker represents one of the most important components in our experiment [2]. It sits just downstream of the electrostatic separator and consists of two pairs of 0.75 m long by 20 cm wide electrode plates, mounted 15 cm apart. Opposing plates in a pair are biased at $\pm$12.5 kV to deflect the beam into collimators, or to ground to allow the beam to pass undisturbed. The kicker is typically operated at a cycle frequency of $\approx$ 30 kHz (5 μs unkicked, 27 μs kicked) and it will likely be used in "muon-on-demand" mode for the MuCap experiment and possibly for some experiments mounted by the μSR community. Here we provide an extensive report of the work done in 2004 to eliminate the RF emissions reported last year and we detail some of the operational problems and the plans to fix those for the 2005 running. This section was provided by TRIUMF engineers Michael Barnes and Gary Wait, who designed the kicker for our use.

4.1 Elimination of the RF Emissions

The kicker was designed and built at TRIUMF and installed in June 2003 at PSI. Preliminary tests at PSI showed that RF emissions from the kicker severely interfered with experimental detector systems. In addition it was realized by the collaboration that the original specification on the flattop of the voltage pulse was not adequate for this precision experiment. Significant reduction in the RF emissions and improvements in the pulse flattop were required. The kicker was returned to TRIUMF, and extensive changes were made which were based on detailed PSpice modeling of the system. The RF was reduced by a factor of approximately 5000.

The solutions to the RF involved several changes. The most important changes involved gaining a detailed understanding of and then controlling all of the current paths: this was achieved using PSpice together with 3D simulation codes. The elimination of all ground loops was essential. Each cabinet is divided into a controls section, which is in the "quiet" lower part of the cabinet, and a high voltage pulsed section that is located in the upper, shielded, part of the cabinet. The upper section is configured as a Faraday cage. The center of the deflector plate tank is now the star ground point for the entire system. A brass ground plate is installed in each cabinet, as close to the to the deflector plate tank as possible: this acts as a secondary star ground point. Each secondary star ground is electrically connected to the deflector plate tank with RF finger stock. All other internal ground connections, including the ground connections at the base of each cabinet are now eliminated. The high voltage pulses are fed to the deflector plate tank via a coaxial Fischer connector (subsequently replaced) through a hole in the center of each brass ground plate. Where an external cable is fed through a port in the Faraday cage there can be RF noise on this cable. In order to minimize RF noise on cables that must exit the cabinets, these cables exit very close

to the brass ground plate: the cables are strongly filtered, through a very low inductance path, to the brass ground plate.

Improved RF shielding was installed by sealing off leakage points in the doors, screens and various cable feed-through points. The paint was removed completely from all edges of the doors and cabinets. One-inch wide copper foil tape with a conducting adhesive was placed over all the exposed surfaces to prevent rust. Tin plated phosphor bronze wire mesh braid, 0.3 in diameter RF shielding was mounted all around the cabinet door frames. Similarly an aluminum plate, which shields the quiet area of the cabinet from the HV pulsed area, and an aluminum cover plate on each cabinet roof were sealed with the tin plated phosphor bronze wire mesh braid. Each cabinet has two doors each of which had 5 clamps installed so that the closed doors made a good contact at all surfaces. Gasket strips, made of nickel-copper metallized fabric over foam, provided an RF shield for the roof panels and were also used to provide a good contact between the star ground brass plates and the cabinet wall. Aluminum honeycomb gasket material, 0.125 in wide hole, by 0.5 in thick, was used to replace the aluminum mesh panels in the doors: a factor of 4 between the thickness and the hole diameter provides good shielding. Fans are mounted on one door of each cabinet on the outside of the honeycomb panels. The AC power to the fans is fed from the quiet area of each cabinet out through the base of the door, therefore the fan AC power lines do not go into the noisy volume of the cabinet. RF measurements near the surface of the cabinet doors indicated that there was no leakage through the honeycomb; i.e.: the RF meter readings do not increase in the locations adjacent to a honeycomb screen. The honeycomb also has the additional benefit of improving the uniformity of the airflow from the fans.

The configuration of the current limiting resistors was changed: nine 5 in long, 0.75 in outside diameter tubular ceramic resistors, rated at 90 W each, are distributed within each FET stack. Distributing the resistors further reduces the RF generated. These tubular resistors, which have an inside diameter of 0.5 in, are mounted on the side of each FET stack. In order to minimize the inductance of the FET stack, and hence the magnitude of overshoot for a given capacitive load and current limiting resistance. The current through each resistor returns through an insulated conductor mounted in the inside diameter of the resistor (i.e. a coaxial structure). Each resistor has a value of 24 Ω (216 Ω per stack): this value was chosen because PSpice calculations showed that the overshoot is reduced to 2%, lasting for $\approx$ 70 ns, without unduly increasing the 10% to 90% field rise and fall times.

4.2 New Flattop Circuit

A new "flattop circuit" consists of two 220 nF, low inductance, capacitors separated by a "compensation FET". When the FET stack is off, the associated compensation FET is turned on and therefore both 220 nF capacitors are being charged by the HV power supply. The compensation FET is turned off approximately 50 ns before the FET stack is turned on: hence only the second 220 nF capacitor supplies the charge for the 108 pF load and its voltage drops by approximately 490 ppm during the rising edge of the output pulse. However this 220 nF capacitor is not recharged during the flattop of the output pulse because it is isolated from the HV power supply by the off-state compensation FET. Fifty nanoseconds after the FET stack is turned off, the compensation FET is turned on and the second 220 nF capacitor is recharged from both the first 220 nF capacitor and from the HV power supply. The measured waveform, with a 22 μs output pulse at 37 kHz, was averaged over many pulses to reduce background noise. The measured flattop of the pulse is flat to

better than 55 mV in 12.5 kV, i.e., better than 4.4 ppm. The PSpice prediction for the variation of the flattop is 20 mV in 12.5 kV. Prior to the incorporation of the flattop circuit the flattop increased by 0.18% during the pulse. The kicker was re-commissioned at PSI during October 2004.

4.3 MOSFET Card Failure and Solutions

Recent failures of MOSFET cards are believed to be attributable to several reasons:

- Breakdown of a connection between the Fischer connector and deflector plates, with the beam pipe, due to out gassing of the cable insulation.
- Breakdown within a Fischer plug, on the output of a modulator: "sealed environmental" plugs were incorrectly ordered and the sealed plugs were not correctly wired.
- Timing problems of the MOSFET cards.

The MOSFET cards are not designed to be able to turn-off high current; doing so on a repetitive basis causes the MOSFETs to avalanche, quickly destroying the MOSFETs. The occurrence of the first two items, at high repetition rate, causes the MOSFETs to turn off a high fault current (up to 54 A) and therefore results in destruction of the faulted stack of MOSFETs. It is planned to incorporate an interlock in the system to help to prevent the MOSFETs being turned off while high fault current is flowing; this should be effective in 95% of such faults. Timing problems with MOSFET cards can result in a MOSFET avalanching during normal turn on: at a high repetition rate this MOSFET is quickly destroyed. Destruction of the MOSFET by avalanching has, in all tests conducted at TRIUMF, resulted in the gate-source of the MOSFET failing to a short circuit. This is consistent with the failures seen at PSI. In several instances, timing mismatches, and hence failures of MOSFET cards, are known to be due to damaged fiber optics. These fiber optics will need to be replaced. The MOSFET cards have been returned to TRIUMF and will be tested to determine whether there has also been any timing drift of the fiber optics on the cards. In order to make the MOSFET cards more insensitive to timing mismatches, it is planned to incorporate a gate resistance of approximately 3.7 Ω on the gate of every MOSFET. This gate resistance will slow down the turn-on voltage collapse across a MOSFET, from approximately 3 ns to 6 ns, without significantly (less than 1 ns) increasing the deflector plate voltage rise time. The gate resistance reduces the maximum drain-source voltage across a MOSFET, during turn-on, which can result from a timing mismatch; therefore the MOSFET is less likely to avalanche. However extreme care must still be taken to avoid damaging fiber optic cables. Tests at TRIUMF, on individual MOSFETs, also show that the turn-off voltage rise time is increased by having a gate resistance and hence an individual MOSFET can turn off a relatively high current without avalanching. Tests at TRIUMF showed that without a gate resistor, an individual MOSFET would fail after only ten pulses when attempting to turn off 40 A but with 3.3 Ω of gate resistance it could: a) turn off 50 A and survive for more than 8,000 pulses (test stopped at this point) providing the average power dissipation was kept low; b) turn off 60 A and survive for more than 1,000 pulses (test stopped at this point) providing the average power dissipation was kept low.

All the MOSFET cards will need to be re-timed after the gate resistance is added.

5 Detectors

5.1 Entrance Muon Counter

The Entrance Muon Counter (EMC) is a wire chamber positioned at the end of the beampipe, where the muons enter the ball (see Fig 4.) It records the time and position of muons entering the detector. The beam profile provided by the EMC is used for the purpose of focusing the beam. The information on the time of incoming muons allows us to study and possibly reject fills in which a muon entered the detector during the measurement period. The EMC must function with an instantaneous beam rate of up to 10 MHz.

The EMC is filled with a gas mixture of 70% CF4 and 30% isobutane. It has 25 μm aluminized Mylar windows at the front and back. There are two planes of 20 μm diameter tungsten wires, one in the vertical and one in the horizontal direction. There are 100 wires on each plane with 1 mm spacing. The wires are connected together in pairs for readout to reduce the number of channels, thus the detector has 2 mm resolution. The wire planes are separated from the outer windows and each other by 12.5 μm aluminized Mylar sheets which are at a positive high voltage. The chamber is read out by six CMP16F amplifier/discriminator boards which produce logic pulses between 40 ns and 100 ns long depending on the analog pulse time over threshold.

In the 2004 run the EMC was run at 3.0 kV. At this voltage it had an efficiency for detecting muons of approximately 98%. A higher efficiency could have been obtained by increasing the voltage but 3.0 kV was used in order to minimize the efficiency for detecting decay electrons. A beam profile from the EMC can be seen in Fig. 5.

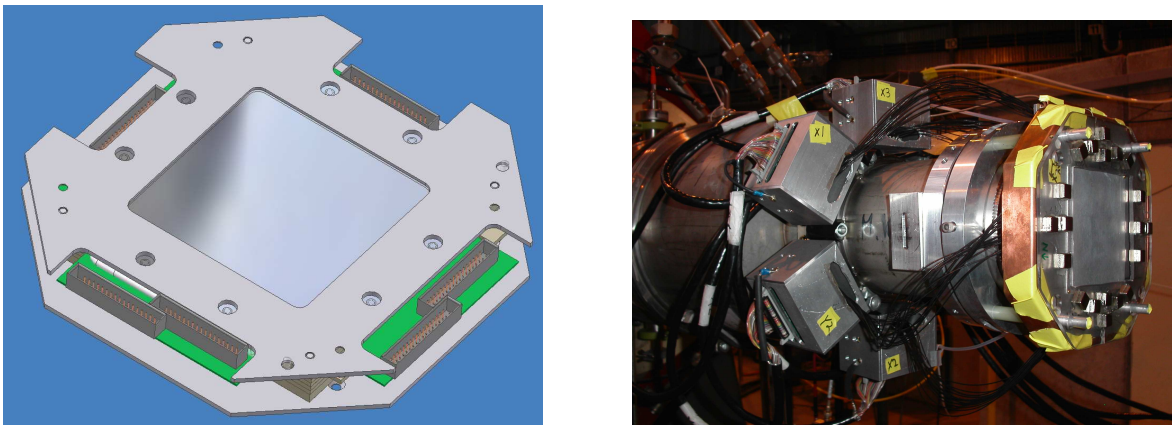

Figure 4: *The entrance muon counter(EMC) is a wire chamber designed to handle high beam rates. Left: A CAD drawing of the EMC. Right: The EMC mounted on the beampipe. The magnets used to create a 50 Gauss field in the EMC are visible on the front face.*

5.2 Tiles

The MuLan ball was fully commissioned during the fall 2003 run and used successfully. During 2004, a few problems were identified and addressed. Many detector elements occasionally produced pulses that were very distorted from the standard scintillator/PMT pulse shape. This was tracked down to electrical discharges to the mu-metal via the conducting glue used to hold the acrylic to the

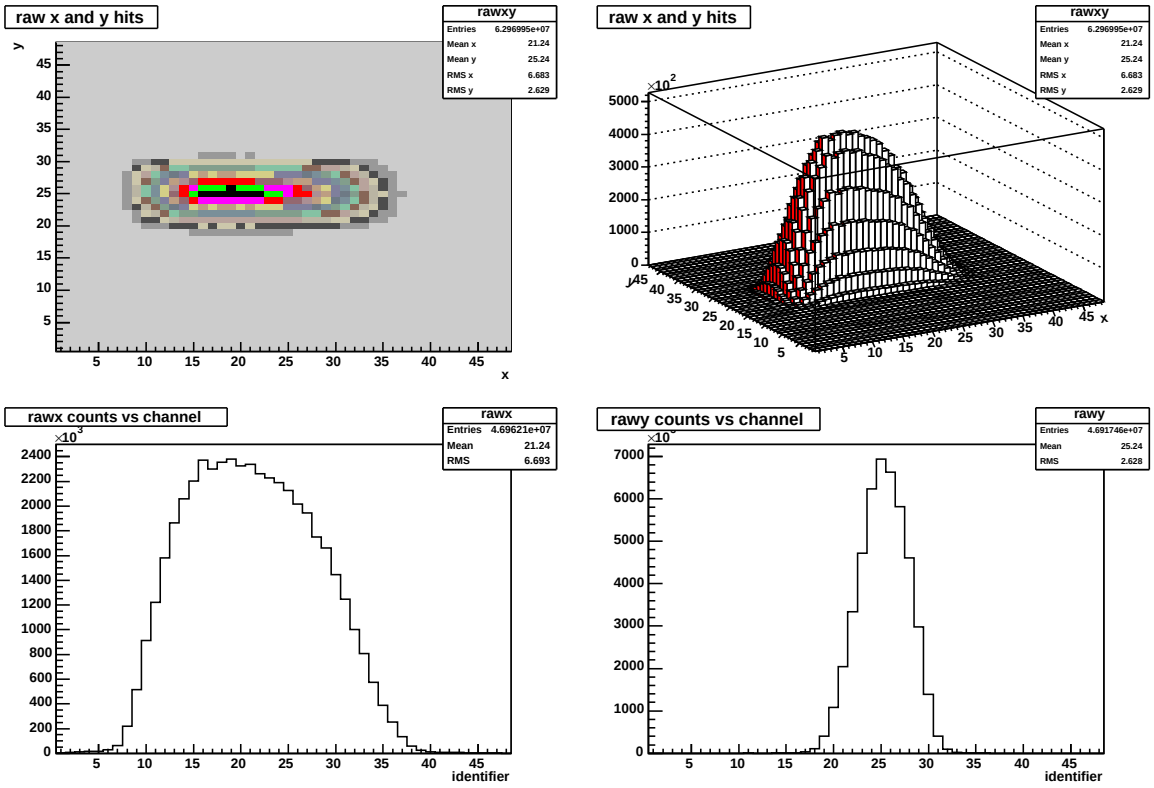

Figure 5: *Several views of the beam profile from the EMC. The top two plots show the two dimensional profile while the bottom two are the horizontal and vertical profile separately. The units are EMC channels, which are 2 mm. At the EMC the beam is 13.4 mm wide in X and 5.2 mm wide in Y .*

PMT. We systematically removed the glue from each of the 340 detector elements and reassembled the detector. Additionally, the scintillator pulses were on the order of 15 ns wide (full-width 20% max) , so to reduce dead time we chose to implement clip lines. These were installed at the base of the PMT and the resistance was tuned to produce pulses that were 9 ns wide (full-width 20% max). The entire detector was then prepared for data taking by undergoing a calibration procedure. We developed a program that varied the high voltage and determined the average pulse height on our digital oscilloscope. It then recorded the pulse heights as a function of high voltage and determined the appropriate setting to produce a 400 mV pulse. Since the MuLan detector is highly segmented, there are many possible failure modes. We encountered various analog signal cables and high voltage cables that had problems when we first installed the system. There were two detectors that caused problems intermittently and were replaced. The other 338 tiles on the ball functioned perfectly throughout the run.

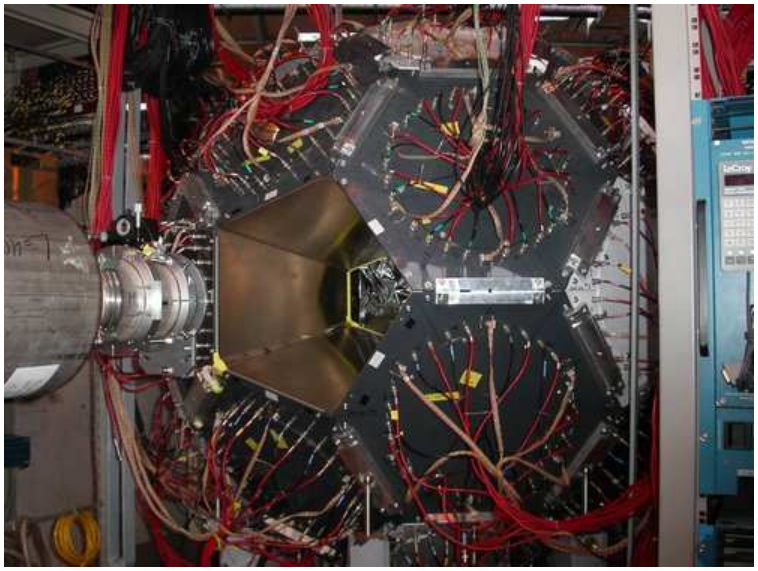

Figure 6: *A picture of the MuLan ball installed in the $\pi E3$ area.*

6 Helium Bag, Targets and Magnets

Special care was taken to minimize the amount of material in the path of the muons upstream of the stopping target. The beam exited the vacuum through the 9.3 cm diameter, 76 μm-thick, Mylar vacuum window that was built for the MuCap experiment. It then passed through the EMC (described above) and then entered a helium bag, which spanned the space between the EMC and the target.

Two physics targets were used in the run: Arnokrome-3 (AK-3, an alloy with a very strong internal B-field) and sulfur, which is well known for its small residual polarization. A new target assembly, installed inside the ball, supported the targets and permitted rotation and tilting with respect to the vertical plane. Figure 7 shows the new, enlarged AK-3 target mounted inside the MuLan ball.

The AK-3 has a strong internal field and its orientation was regularly changed throughout the run. Sulfur is used because the muons are 90% depolarized after stopping in it. A permanent magnet array surrounds the sulfur disk. The magnets are configured to produce a dipole of ≈ 150 G in the central stopping region. This field rotates the muon spin with a period of roughly 500 ns. In addition to these targets, a non-depolarizing silver disk was used with DC (unkicked) beam to rapidly acquire data having a very high asymmetry in each tile element. Analysis of this data provides the initial muon polarization vector to good precision.

A small fraction of incoming muons — roughly 1 in 1000 — will stop in the EMC foils. Special runs were taken with a plastic foil located on the downstream side of the EMC to enhance this effect. The foil was thick enough to stop the entire beam. Because the magnetic field at this location was unknown and arbitrary, we built a second, permanent magnet array (visible in Fig. 4) to produce a field of approximately 50 G in the center of the EMC foils. This magnet's orientation was also systematically rotated throughout the normal data-taking period.

Figure 7: *View inside the MuLan ball of the new target assembly and helium bag. The target is a large sheet of AK-3 and, in this photo, the helium bag is not fully inflated. The beam enters from the right.*

7 Electronics

7.1 Discriminators and TDCs

There have been delays in the waveform digitizer boards that we had planned to use to readout the detector. So, we chose to use a set of discriminators and TDCs to record the detector signals. We opted for the 16 input, CAMAC style, Lecroy 3312 and 4413 model discriminators because they can be densely packed, have good timing characteristics, and were available. The output of these modules were sent to CAEN V767 multi-hit TDCs which have been discussed at length in Ref. [1]. To accommodate the input width requirements of the TDC, the discriminators were set to give a minimum pulse width of 10 ns to facilitate pileup reconstruction.

We used a waveform digitizer from the Brookhaven $g-2$ experiment to determine the best value to set the threshold. Using a linear gate, we were able to record only pulses that had been discriminated. This allowed the determination of pulse area as a function of threshold. In order to reduce systematic effects associated with threshold or gain changes, it is important to be at the local minima seen in Fig. 8. We choose a threshold of 200 mV.

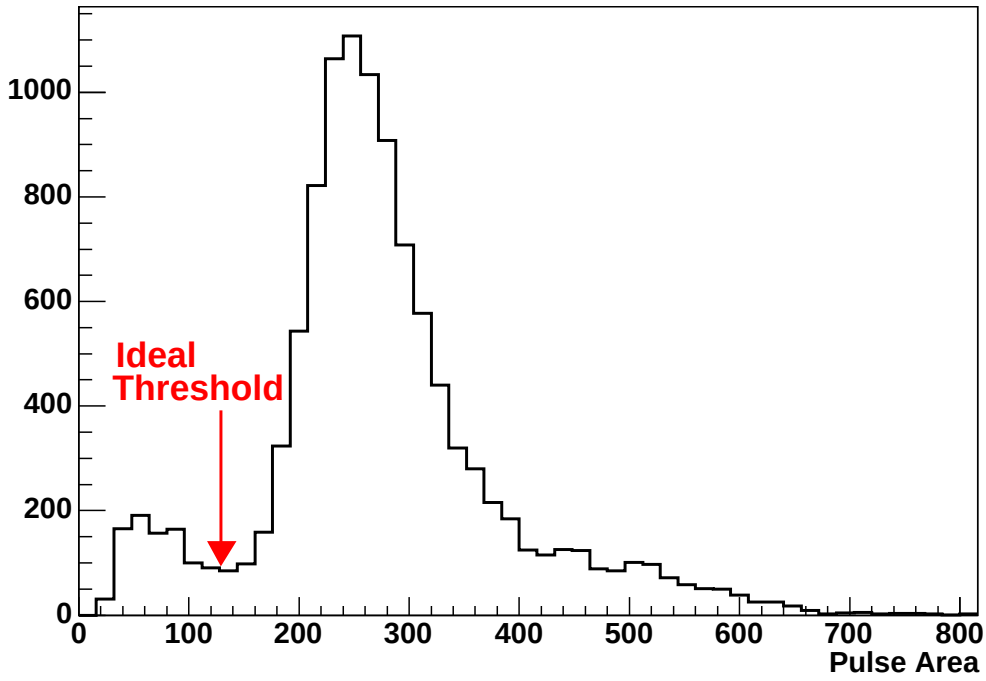

Figure 8: *Plot of the area of PMT pulses from a single tile. The MIP peak is obvious. The threshold is set at the minimum between the MIP peak and the background.*

7.2 Clocks and Timing Control Systems

Although MuLan is driven by the control of systematics, the timebase of the experiment is not expected to be a major concern. Frequency synthesizers with absolute timebase accuracy and stability at the 0.1 ppm level are readily available from commercial vendors; for the master, high precision timebase of MuLan and MuCap experiments, we have obtained and utilized an Agilent E4400 synthesizer, which is in this equipment class.

In long term tests in early 2004 utilizing a high accuracy, recently calibrated Hewlett Packard 5385A Frequency Counter, the absolute frequency and differential frequency drift of the E4400 were both determined to be below the 10^{-8} level. A number of cross-checks with other high frequency clock sources in 2003 and 2004 show that the common mode clock/counter drift was at or below the same level. Similar checks were performed during the fall 2004 run; no deviation of output frequency from the demand value was observed. The demand frequency itself is unknown to most of the collaboration so that the analysis remains "blind"; a record of the actual demand value is kept by a small group of MuLan and MuCap collaborators, and will be revealed to the analysis group when they have finished their studies.

In addition to the (approximately) 200 MHz master clock, there are a number of other independent, lower accuracy clock sources in the experiment. These include

1. The DAQ segment clock, which imposes synchronization signals to align the data across the

multiple MIDAS front end computers. A gate generator provided these signals, with start pulses generated by the master front end computer. This gate was triggered at about 100 Hz.

2. The DAQ rollover clock, which generates data for the CAEN MTDCs at a rate to ensure that clock rollovers can be properly reconstructed. The period of this clock must be less than half that of the MTDC rollover period, but should not otherwise be synchronized to it. This clock was generated by a self triggered gate generator, at approximately 2.5 kHz.

3. The kicker cycle clock, which generates the timing waveforms for controlling the kicker and the associated fill and veto marker pulses which feed the discriminator banks. While these pulses were generated at the hundred kilohertz scale, the underlying FPGA-based programmable pulse generator (PPG) was clocked at approximately 42 MHz.

The frequencies of the PPG and master clocks were chosen such that beat frequencies between these clocks and the beam RF would not produce Fourier peaks that would interfere with expected structures in the analysis (such as the kicker cycle and muon lifetime scale). We therefore have no reason to expect that these clocks will give rise to any systematic effects.

7.3 LED Calibration and Testing

An LED is mounted on each of the photomultiplier tubes on the MuLan ball. Fast light output (few nanoseconds) is made possible by a triggering circuit mounted with the LED and embedded in the detector housing. A driver circuit controls these individual LED pulsers. This circuit provides power and the trigger pulse that produces the light flash. The trigger pulses are generated in a VME-based programmable pulser called the flight simulator. Pulses from the computer controlled flight simulator are routed along with the power to each LED by a driver box.

Twelve driver boxes were constructed and installed during the summer of 2004. Each box controls 32 LED pulsers. At the end of the summer installation period all of the cabling to the detector was complete and 6 of the 12 boxes were fully operational. A database with a web interface was added in order to simplify control of the LEDs and allow for changes in the configuration when necessary. The database/web interface was successfully linked with the MIDAS based DAQ.

Several problems were encountered during the process of installation and testing. Individual channels would sometimes fail. Although the problems could be corrected, the source was not determined and remains under study. The LED system was used occasionally during the fall 2004 running period and typically only a few channels were fired during the tests. The system functioned as expected under these limited tests.

During the upcoming year the remaining six driver boxes will be brought into full operation. The system will be strenuously exercised and the performance will be better characterized. The system will be used, out of beam, to provide a data source for the new waveform digitizer installation.

8 Data Acquisition

During 2004 our DAQ efforts were focused on the development, commissioning and running of the data acquisition for the fall 2004 pulsed beam run. The DAQ provided readout for

- The CAEN multi-hit TDCs instrumenting the 340 tiles of the MuLan detector ball and 96 channels of the entrance muon counter.

- Several $g-2$ waveform digitizers instrumenting a few representative scintillator tiles.

In addition, the DAQ provided the control and readback for the high voltage, electrostatic kicker and other beamline elements, and the operation of the LED pulser system on the MuLan ball detector.

The DAQ is based upon a local Gigabit network of several frontend processors, one backend processor, and redundant disk arrays for large-scale data storage. We developed the DAQ with a modular design philosophy and the MIDAS software package. The DAQ was organized to accumulate the data in continuous chunks or time segments with fixed lengths of about 10 ms. This permitted the accumulation of data without deadtime by utilizing the on-board memory in VME hardware for intermediate storage of incoming data. Between each time segment the frontend computers were responsible for completing the readout of the data fragments and sending the fragments over the Gigabit network to the backend processor. One frontend was denoted the master, and assumed the responsibility for synchronizing the acquisition cycles across the various frontend processors.

Three separate frontend processors were responsible for the high rate data-streams from the VME crates that instrumented the scintillator tiles, entrance muon counter, and waveform digitizers. The muon counter frontend permitted storage of both raw hit data and derived position/time spectra and the waveform digitizer frontend permitted storage of both raw pulse shapes and derived quantities such as pulse areas, pulse widths, etc. Of great importance for data integrity, our CAEN multi-hit TDC routines were designed to continually monitor and automatically reset any errors from buffer overflows, clock synchronization, etc., that were reported by the hardware. The backend processor was responsible for the merging of the data fragments from the different frontends and the transfer of the assembled events onto the disk arrays. It also managed the user control via the MIDAS web interface and the MIDAS online database. The backend analyzed a portion of the data in real time, giving online diagnostics for beam spot size, kicker efficiency, and detector health. The large volume of incoming fragments and outgoing events demanded a dual processor machine for the event building and 1 Gigabit network switch for the data transfer.

Data storage for the fall 2004 run was provided by six RAID5 redundant disk arrays with available space totaling 8.25 TB. The arrays were physically mounted in four separate, dual processor rack-mount computers. Each of these computers were connected to both our internal Gigabit Ethernet DAQ network as well as the PSI network, and doubled as our immediate offline data analysis cluster. The MIDAS lazylogger task ensured that we had a complete backup of our data on the PSI tape archive in the unlikely event of catastrophic RAID failure.

During the fall 2004 run we accumulated data at a time-averaged incident muon flux of typically 300 kHz and a usable decay positron rate of typically 130 kHz. The corresponding data rates were about 4 MB/sec from the scintillator tile frontend and about 6 MB/sec from the entrance muon counter frontend. Under these running conditions the DAQ livetime was typically 85%, and generally it operated quite smoothly. The design, development, and commissioning of the data acquisition was the Master's research project for Kentucky graduate student Santosh Cheekatmalla. Mr. Cheekatmalla successfully defended his research project in December 2004.

A number of DAQ tasks are still required to complete an acquisition that can handle both a full array of 500 MHz waveform digitizers and a fivefold increase in incident beam flux. Our plans are for commissioning of the waveform digitizer readout during spring 2005 at Kentucky and during summer 2005 at PSI. This work will focus on developing and debugging the communications

between the acquisition software and the waveform digitizer, and testing the algorithms for fitting and parameterizing the raw pulse shapes from scintillator tiles. In addition, a new scheme for either hardware compression or hardware pre-scaling of the raw data from the muon counter during the beam-on period is necessary to permit running at considerably higher muon fluxes. For future runs with much greater data volumes we will use an LTO tape system for archival storage and our RAID systems for smaller-scale "online" analysis and data storage.

9 Waveform Digitizer Progress

In 2005 the PMT signals will be read out by 500 MHz waveform digitizers. From the waveform record, we extract the time of arrival and energy deposited for each decay positron. Although, multihit TDCs may provide adequate timing, time and gain stability; pileup, noise, correlations between channels, etc., are much easier to investigate and understand with a waveform digitizer.

The conceptual design of the MuLan waveform digitizer is very simple. PMT signals pass through a amplifier buffer into a 500 MHz Flash ADC (FADC). Two 8-bit samples from the FADC are sent to a Field Programmable Gate Array (FPGA) every 4 ns. If the signal is over a selected threshold (either digital or analog) the data is written to a FIFO. At regular intervals, front end processors read out the FIFOs at one end, during which time the FPGAs can continue to write data in at the other.

After building a very successful initial prototype, which demonstrated that we could handle the high data output of the FADC, we completed our first full prototype in late summer of 2003. Progress on the prototype was slow at first. For several months, a bug in a vendor-provided FPGA simulation tool prevented systematic debugging of board input/output through the VME bus, our principal means of examining the board's internal behavior. After changing the software, we soon demonstrated that we could do most VME operations, including communication between the VME interface and the large FPGA which is assigned to reading, reformatting and sending out data to the FIFOs. We learned also that our JTAG-EEPROM and EEPROM-FPGA connections, essential for initial programming, were working correctly. Power and cooling were both adequate. General purposes NIM I/O ports on the front panel worked successfully. Address relocation also worked.

However, because of a design flaw in the clock distribution network, we were unable to perform any successful waveform sampling tests or block reads of the FIFOs. A schematic error on the flash ADC pin assignments likewise made waveform sampling tests impossible.

Although we learned a great deal from our first full WFD prototype, we decided that correcting the errors in that prototype would be more cost and time intensive than a completely new layout. This new prototype was delivered in early December 2004. There are now two Xilinx Virtex II FPGAs reading out the four Flash ADCs on each board. Although we only used a small fraction of the gates in the original single FPGA design, the clock management resources were fully utilized, making the placement and routing of new features increasingly difficult. The extra FPGA has also led to a cleaner and simpler bus layout. Additionally, we have replaced the Xilinx Spartan II FPGA that was originally used to implement the VME interface with the same type of Virtex II FPGA that we are using for Flash ADC readout. The new part allows us to use a higher clock rate to synchronize VME operations, lowering transfer latency and increasing VME bandwidth. The switch to three Virtex II FPGAs has required us to redesign the power regulation and distribution circuits to support the higher current requirements. Tests on the new board have been underway for several weeks. There will be further updates at the PAC meeting.

10 The 2004 Data Set and Analysis Plans

In the first half of 2004, our analysis team focused on data taken the previous year. This data was obtained with a DC beam of various rates and on several different targets. The intention had been to produce our first precision muon lifetime value, but it became obvious that the data was more useful in determining potential systematic problems associated with our electronics, data acquisition system, targets, and detectors. Based on findings from this data, we changed several components of the data acquisition, added clip lines to the PMTs and determined the average local magnetic field of the AK-3 target to be 4300 Gauss.

During fall 2004 we collected a new data set, this time with a kicked beam in addition to DC. Data was collected with a variety of conditions, varying the incident muon rate, kicker voltage, target, and several other parameters. We estimate that we collected over 4×10^{10} positron decays during the measurement period, with about 1×10^{10} using a sulfur target and 3×10^{10} with an AK-3 target. This should give us several statistically independent determinations of the muon lifetime with a total uncertainty of less than 10 ppm. Figure 9 shows a lifetime fit to a small subset of the data, equivalent to a 10 minutes of data taking. The histogram has a shape similar to a charging and discharging capacitor corresponding to our accumulation and measuring periods respectively. It is fit with a simple three parameter function ($f(t) = N \exp^{-\frac{t}{\tau}} + B$) where the amplitude N, lifetime τ, and background B terms are allowed to float. The background term accounts for muons that enter the detector during the measurement period and other uncorrelated events such as cosmic showers.

We have subdivided the analysis effort this year. There is a team focussed on preparing and processing the raw data for making histograms. Another group is scrutinizing this processed data, fitting the histograms, and searching for problems. Finally, there is another group that is working on quantifying systematic errors in the data. There is much overlap between these analysis teams in personnel and topics, but we feel that this approach will lead to a correct determination of the muon lifetime in the shortest possible time. This will be a blind analysis. The master clock frequency is unknown to all but one collaborator, who will not be working on the analysis.

In determining the lifetime value, there are many consistency checks that can be performed. Each of the 170 detectors will be fit individually to check for any geometric dependency. (See Fig. 10 for example.) We will compare the results obtained from the sulfur target with that of the AK-3. In addition, the magnetic field orientation was changed on a regular basis, so we can compare the data sets of each orientation for consistency. We will check for any dependence on the background level by comparing sets of data with different kicker voltages. All of this is in addition to some of the standard studies we expect to perform such as fit start/stop time studies, bin size studies, and differences in histogram filling algorithms (see Fig. 11 for example).

A portion of the run was spent studying various systematic effects. The following is a list of some of the known issues with a simple explanation of what we measured and how we expect to quantify or minimize the effect on the lifetime value.

- **Pileup** – Measuring the width of the discriminator pulses will allow a careful determination of the number of missed events due to pileup. We will use a pileup estimation method, where we check for events a fixed time after every original event and use that information to estimate the number of events that went undetected due to pileup. Also, data was gathered at very high beam rates (∼10 MHz) for a portion of the run in order to magnify the effect of pileup for closer study.

- **Gain and Threshold Changes** – We used the $g-2$ waveform digitizer to monitor several detectors in order to quantify the change in gain and threshold during the measurement period. We also maximized the effect of these changes by taking dedicated runs with the discriminator threshold set at the peak of the MIP spectrum.

- **Background Stability** – Several measurements were performed to observe how the beam rate changed with kicker voltage and measurements of the kicker voltage stability were performed. This allows us to calculate the effect of kicker instability on our measurement. Initial estimates indicate that the effect is significantly smaller than our statistical error for this run. In addition, the EMC will be used to check for changes in the incoming muon rate during the measurement period. Finally, we had a scintillator detector, that was outside the beamline, with a Sr^{90} source on it which acted as a random counter. The events in this detector will be plotted relative to the ones in the main detector to insure that we have a flat distribution.

- **Polarization Effects** – We took some data with a silver target to determine the initial polarization of the muons in the beam. This will assist in determining the best way to minimize the effects of any residual polarization in our targets. The symmetry of the detector cancels the effect of polarization changes to a large degree. And magnetic fields at the target and the EMC are designed to cause precession frequencies fast enough that they will not effect the lifetime measurement.

11 Beam Request 2005

A modest physics data set has been obtained in 2004 that will permit thorough analysis, a thesis for one student, and possibly our first physics publication. Although our online analysis suggests that the concept of the experiment is sound, only a full offline analysis, complete with systematic studies, will be able to reveal if any hidden problems exist. We intend to give the analysis effort very high priority in 2005.

The MuLan detectors (ball and EMC) are tested and ready for a full production run. We will expand the LED system coverage but no significant changes are otherwise anticipated. The beamline has been thoroughly investigated, but we still feel there is room for minor optimizations, especially related to the extinction factor. The kicker system performed well but had reliability problems that are being addressed. Repairs and stress tests will occupy the first few months of 2005. The custom waveform digitizers are being debugged at the time of this submission. Given the extensive studies of this prototype, we anticipate that this is the final prototype and that full production will follow a short test program. We expect a small subset of WFDs by April 2005, and the full production a few months later. The DAQ system has worked quite well given the demands of a CAEN-TDC-based data stream. Although much code has been written in anticipation of a WFD-based data stream, this part of the system remains incomplete until the hardware is available. We anticipate testing this system using the LEDs in late spring 2005.

This summary, together with consultation with the other primary users of the πE3 beam area, leads us to suggest a schedule as shown in Fig. 12. It features 3.5 weeks of testing and studies at the beginning of June in which the primary purpose will be to test part of the system with both WFDs and CAEN TDCs in parallel. Additionally, this time will be used to carry out final beam tune optimization studies, and to test one or more candidate target materials. Following this period, we

will need to replace all of the CAEN-TDC electronics chain (discriminators, CAMAC crates, logic) with the new VME-based WFD system. To do so and to then test the new online software, and its critical real-time compression scheme, will require roughly a two month interlude. Therefore, our next beamtime request begins in mid-September. We have requested 5.5 weeks during this period with the purpose of tuning up the system and taking $3-4$ weeks of full production data. We anticipate that such a data set will be a major step forward and will require considerable analysis time prior to our 2006 full production run aimed at 1 ppm precision.

References

[1] D.W. Hertzog *et al.*, MuLan Progress Report 2003.

[2] M.J. Barnes and G.D. Wait, IEEE Trans. Plasma Sci. **32** 1932 (2004).

[3] PSI Graphic Transport Framework by U. Rohrer based on a CERN-SLAC-FERMILAB version by K.L. Brown, D.C. Carey, Ch. Iselin and F. Rothacker: Transport, a Computer Program for Designing Charged Particle Beam Transport Systems: CERN 73-16 (1973) and CERN 80-04 (1980).

[4] PSI Graphic Turtle Framework by U. Rohrer based on a CERN-SLAC-FERMILAB version by K.L. Brown, Ch. Iselin, D.C. Carey: Decay Turtle, CERN 74-2 (1974).

[5] J.F. Ziegler, J.P. Biersack and U. Littmark, Stopping and Range of Ions in Matter, Pergamon Press, New York, 2003. SRIM program available for download at http://www.srim.org/.

[6] K. Halbach, Nucl. Inst. Meth. **169** 1 (1980).

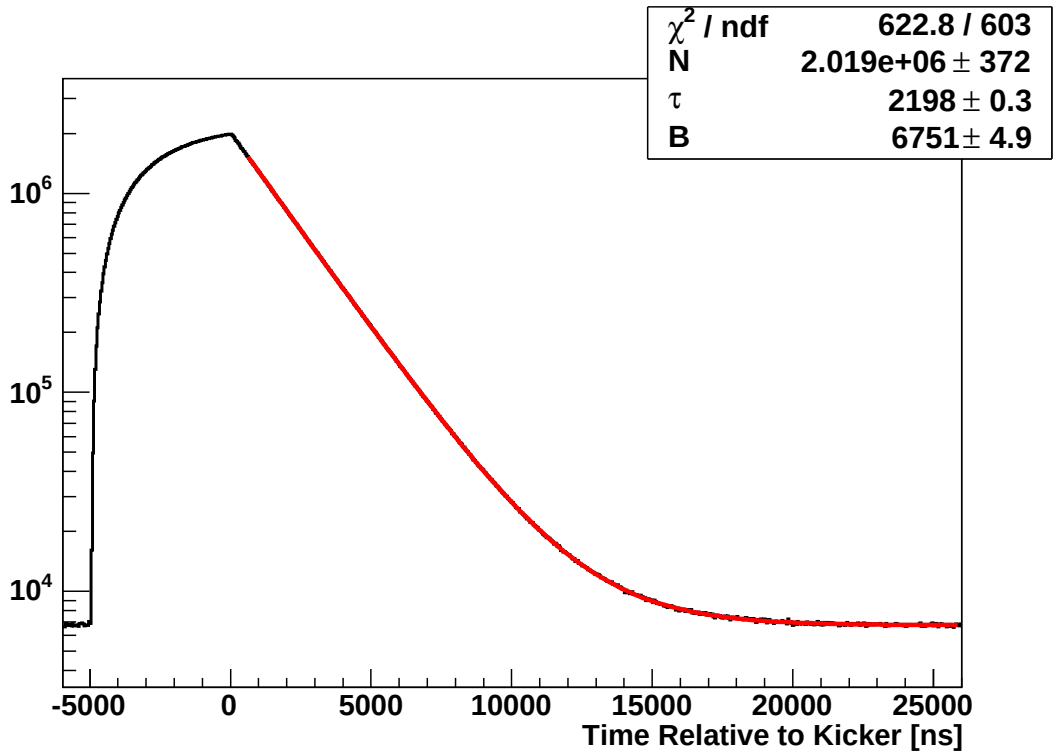

Figure 9: *Example of a lifetime fit for data equivalent to a single 10 minute run. For the 5 μs before the kicker turns on muons are entering the ball. The time scale includes a secret offset.*

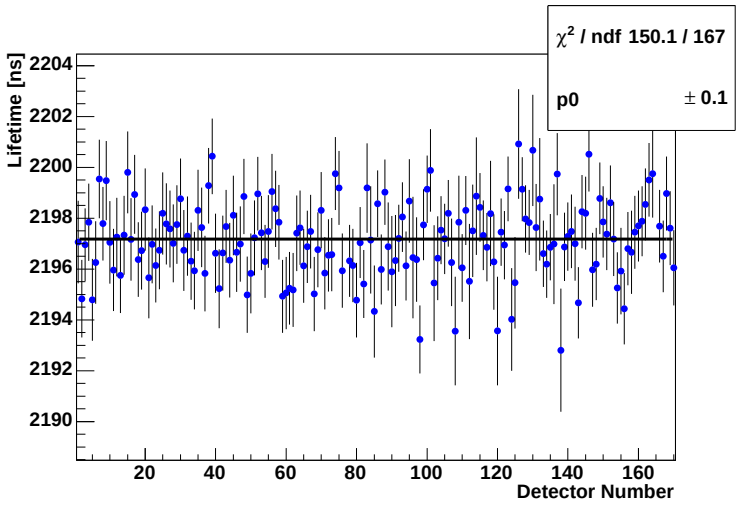

Figure 10: *Measured lifetime for each of the 170 tile pairs for a subset of the data. Each detector is fit individually with a three parameter function and the lifetime results are plotted on the same graph. Here the distribution of measured values is fit with a constant showing consistency between the detector elements. The time scale includes a secret offset.*

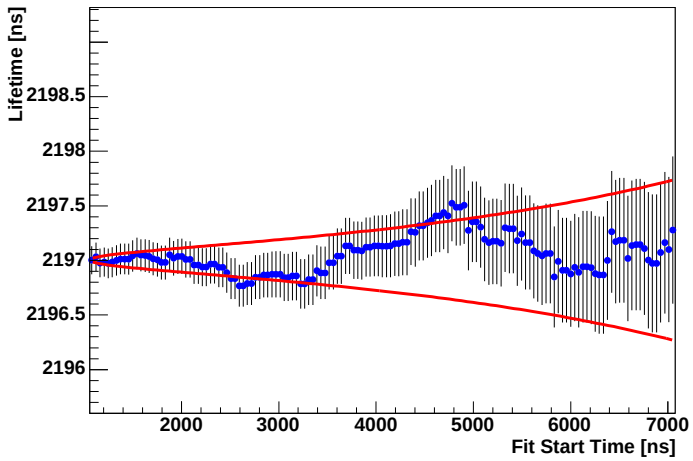

Figure 11: *Measured lifetime versus start time of the fit. The sum of all detectors is fit with a three parameter function many times, with the start time of the fit increasing by the bin size of the histogram. This plot shows the measured lifetime with start times from 1 to 7 μs. The red bands show the expected one sigma statistical deviation of any point relative to the earliest measurement. The time scale includes a secret offset.*

Figure 12: Snapshot of the proposed beamtime request of the MuLan experiment. This was prepared in consultation with the MuCap and ALC groups, who are also primary users of πE3.